PERGAMON

Chemical Engineering Science 56 (2001) 5653–5661

Chemical Engineering Science

www.elsevier.com/locate/ces

The application of the multi-pass rheometer for precise rheo-optic characterisation of polyethylene melts

K. Lee, M. R. Mackley *

Department of Chemical Engineering, University of Cambridge, Pembroke Street, Cambridge CB2 3RA, UK

Abstract

This paper presents an overview of the application of the Multi-Pass Rheometer (MPR) for the study of polymer processing with particular reference to flow birefringence measurements. The MPR is a two-piston capillary rheometer recently developed at the University of Cambridge. We review previous experiments that have been carried out on molten polymers using the MPR and we report on recent results of flow birefringence experiments for a polyethylene (PE) melt. Using a specially designed optic flow cell, molten PE was passed within a Double Cavity Die. A field-wise flow-induced birefringence technique was used to obtain the stress field in a complex flow of a flowing molten polymer. In general, for the PE tested, the entry stress field in the second cavity was found to be different from that in the first. The differences observed in the overall entry stress fields in the two slit configuration could be explained as resulting from the extensional and shear strain history experienced by the polymer. We have carried out matching K-B.K.Z.–Wagner numerical simulations and found that reasonable consistency can be achieved for certain polymers. As a consequence of these experiments, we have found that the MPR is a very good platform for experimental flow birefringence studies that can be matched with numerical simulation and in addition experiments can be carried out with small 20 g quantities of material.

Keywords: Polyethylene; Double-cavity die; Strain history; Multi-pass rheometer; Flow birefringence; Wagner model; Viscoelastic

1. Introduction

This paper is concerned with the development of a laboratory scale apparatus that can be used to evaluate the processing behaviour of relatively small quantities of molten polymer. The Multi-Pass Rheometer (MPR) has been under development in Cambridge for the last 5 years (Mackley, Marshall, & Smeulders, 1995). The machine has two servo-hydraulic controlled speed pistons, and is capable of measuring processing performance and generating precise, repeatable results under accurately controlled flow conditions.

In its original configuration, it was used solely for rheological measurements for different materials such as ink, paint, chocolate, polymer solutions and emulsions (Wee & Mackley, 1998; Thompson, Mackley, & Nimmo, 2000; Mackley & Thompson, 2000; Engmann & Mackley, 2000; Cheng, Mackley, & Sayer, 2000). For molten polymer, the MPR has been used to study time dependent flow and the effect of pressure on rheological response (Mackley & Spitteler, 1996; Ranganathan, Mackley, & Spitteler, 1999). By using different centre test sections, both rheo-optic (Lee & Mackley, 2000a, b) and rheo-Xray (Mackley, Moggridge, & Saquet, 2000) observations have also been made.

In recent years, there has been considerable activity in the development of different types of polymers using different polymerisation routes (see for example, Martino, 1992; Reade, 1995). Some of these polymers exhibit processing difficulties (see for example, Chowdhury & Moore, 1993) where it is necessary to evaluate the processing performance of these materials when only small quantities of material are available. There has also been major recent advances in the understanding of polymer melt rheology (see for example, Koopmans, 1993; Dealy, 1998) and the numerical simulation of processing flows (see for example, Baaijens, Verbeeten, & Peters, 2000). It is now possible to simulate complex process flows although at this stage it is difficult to have

* Corresponding author. Tel.: +44-1223-334-777; fax: +44-1223-334-796.

E-mail address: mrml@cheng.cam.ac.uk (M. R. Mackley).

0009-2509/01/$ - see front matter
PII: S0009-2509(01)00153-1

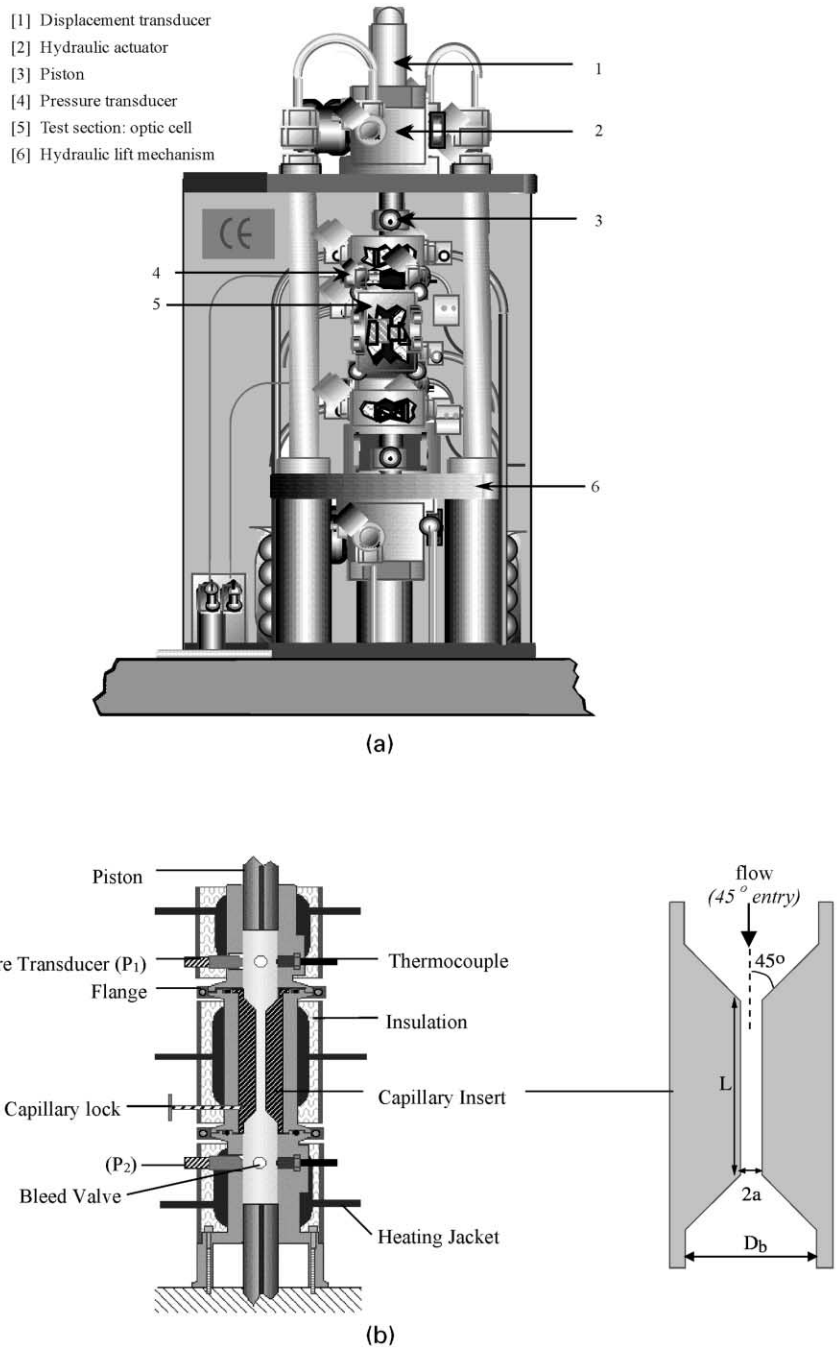

Fig. 1. A schematic diagram of the (a) Multi-pass Rheometer MPR showing full instrument and the optical cell; (b) MPR with a capillary insert. The axial distance between the transducers (P_1 and P_2) is approximately 82 mm, the maximum piston stroke (centre-to-peak amplitude) in a multi-pass is 15 mm and the dimensions of the capillary test section are as shown (barrel diameter. $D_b = 12$ mm, entry/exit flow angle, 45°).

complete confidence in the accuracy of these predictions for commercial processes. The operation of the rheo-optic MPR offers an opportunity to evaluate the performance of these numerical simulations for conditions that are similar to many processing situations and this paper reviews the current status for this objective.

2. The Multi-Pass Rheometer

A schematic diagram of the MPR is given in Fig. 1(a), where both top and bottom piston, test section, hydraulic lift mechanism, servo-hydraulics and pressure transducers are shown. The hydraulic actuator controls the displacement of the pistons and the displacement

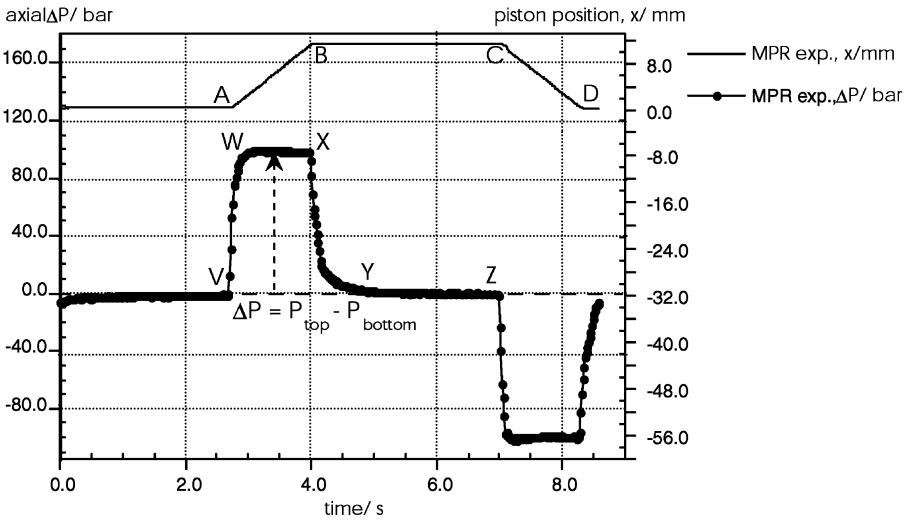

Fig. 2. A multi-pass steady-mode time profile of the axial pressure difference and piston position (piston speed = 8.5 mm/s, piston amplitude = 5.5 mm; and idle time = 3 s). The data was obtained for a LLDPE at a temperature of 190°C using a capillary of ($L/a = 40/2$).

transducers monitor their positions. The main improvement of this machine over the prototype MPR-I is that the polymer resins can be conveniently loaded into the apparatus by lowering the bottom platform/barrel/test section assembly hydraulically.

Fig. 1(b) is a schematic diagram of the MPR fitted with a capillary test section. Either an optic cell (Fig. 3a) or a capillary insert can be used in the centre section. Temperature and pressure are measured on either side of the test section. The distance between the pressure transducers is 82 mm and the length of the test section is 56 mm. The entire system is controlled by a personal computer that executes programs written in LABVIEW™ specifically for control and data acquisition. Data acquisition includes reading piston positions and the pressure traces from both transducers.

The operating modes of the pistons are *steady* and *dynamic*. A description of dynamic mode can be found in Ranganathan et al. (1999). In the steady mode, both pistons are driven synchronously at constant velocity such that fluid in the assembly is driven at steady volumetric flow rate. The operating variables are piston speed, amplitude of piston displacement and total time (in single-pass) or idle time between any two passes. The movement of the pistons can be reversed and repeated any number of times. A typical pressure profile of the MPR steady mode is shown for two passes in Fig. 2, with piston speed of 10 mm/s, amplitude of 6 mm and idle time of 3 s. As illustrated, both pistons are displaced synchronously at constant velocity (A → B) and a rapid pressure difference (V → W) develops across the sample within the test section. A steady state ΔP (W → X) is attained while the pistons are still moving. Pressure relaxation of the material (X → Y) occurs during each dwell time (B → C) and ΔP subsequently diminishes (Y → Z). The remaining profiles were obtained for the reverse motion of the pistons (C → D), hence 'multi-pass'.

In addition, flow visualisation experiments can be carried out using an optic cell (Fig. 3a). The optical set up for flow-birefringence measurements is shown schematically in Fig. 3(b) and the main components are: a Fibreoptics-Heim (model No. LQ2600) light source; a filter and collimating lenses to generate a monochromatic parallel beam (of wavelength $\lambda = 5.14 \times 10^{-7}$ m); and a polarizer and an analyzer oriented at mutually orthogonal positions on either side of the sample, with the polarizer inclined at an angle of 45° to the flow direction. A COHU CCD camera (model No. 4912-5010-0000) detects the *fringes* transmitted through the analyzer. The polarizer, analyzer, collimating lenses, filter and optical mounts were manufactured by Spindler & Hoyer. Quartz optical windows of 15.95 mm diameter and 15.0 mm depth were manufactured with small angle bevels at the edges in order to reduce mechanical stress on the window. Image capturing and recording was performed by a workstation that consisted of a PowerMacintosh G3 with digital video-editing software, Adobe Premiere® 5.1 LE and a Super VHS video set. The flow birefringence pattern was analysed and processed using Adobe® Photoshop® 5.0.2, image-editing software.

2.1. Principles of flow-induced birefringence in polymer melts

In this paper, the flow visualisation comprises *fieldwise* measurement of *birefringence* in order to map the stress field of flowing melt (in the plane of shear gradient). The two most important considerations for the application of the rheo-optical approach are: (i) the sam-

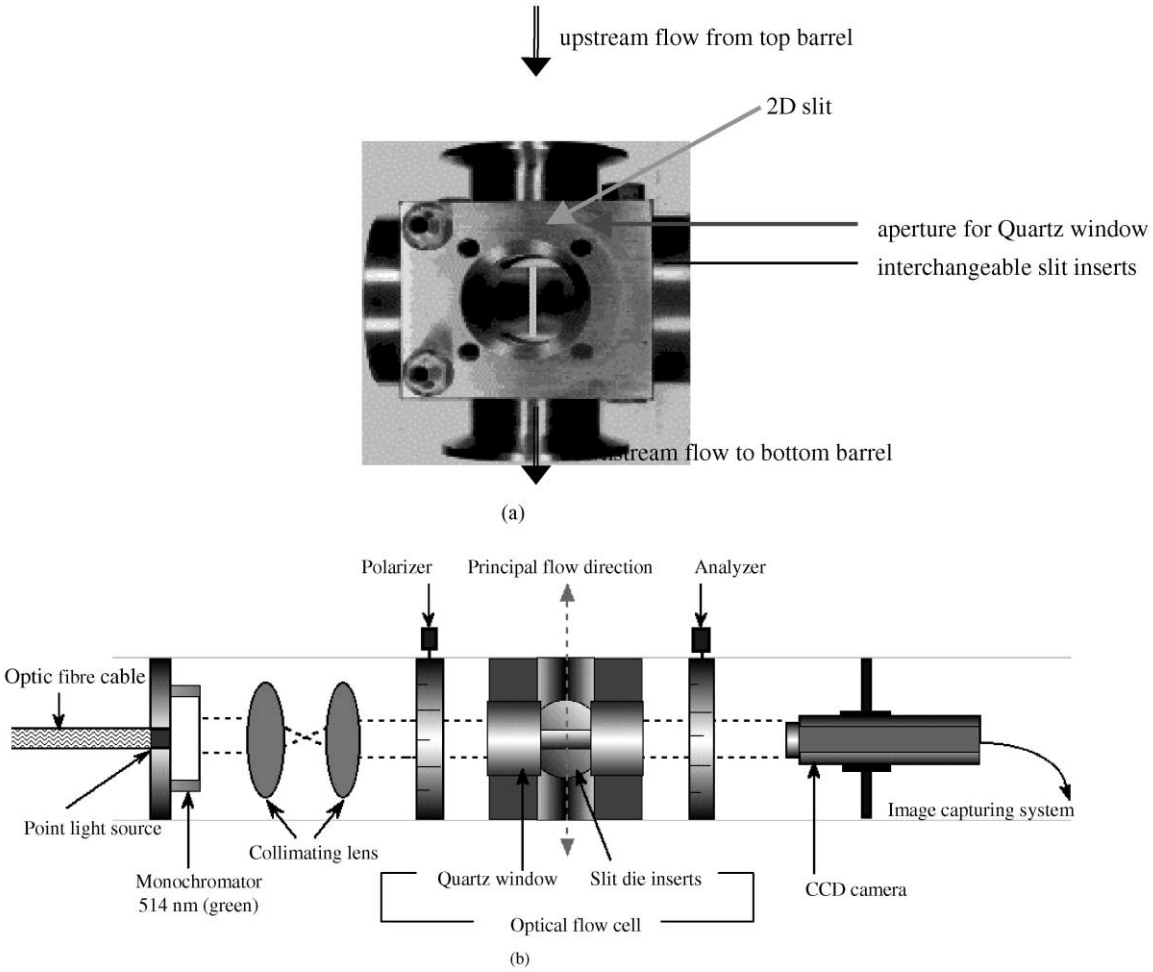

Fig. 3. (a) A stainless-steel optical cell. Shown are the slit inserts, primary flow direction and the aperture for the Quartz optic window (diameter, 15.95 mm and length, 15.0 mm). A schematic of the (b) flow visualisation set up in a MPR for capturing field-wise flow-birefringence.

ple must have suitable optical properties, particularly in terms of transparency and freedom from macroscopic contaminants (this problem can be severe for commercial products); (ii) additional characterisation is often required to establish the relationship between optical and stress properties, for example, with application of the stress-optical rule (SOR) the stress-optical coefficient must be determined (or known a priori). For homogeneous polymer melts, these two criteria are generally fulfilled (Lodge & Macosko, 1994).

The principle of flow birefringence and its application in complex flow study on polymers has been thoroughly discussed (see for example, Baaijens, 1994; Schoonen, 1998). The flow birefringence technique has been a useful research tool in polymer melt rheology and its application is based on an important assumption, the validity of the *stress-optical rule* (see for example, Wales, 1976). This assumption comprises *coaxiality* of *refractive index* and *stress tensors* under all flow conditions. Thus, the *stress* in a deformed system is proportional to a tensor that describes the *orientation distribution* of the polymer *chain segments*; the *refractive index* tensor (also known as *optical anisotropy* tensor) is then proportional to the same tensor, and this proportionality therefore leads to the SOR (Eq. (1)),

$$\Delta n = C(|\Delta\sigma|) \tag{1}$$

which states that the difference in principal values of the refractive index tensor (birefringence, Δn) is proportional to the difference in principal values of the stress tensor, $|\Delta\sigma|$. The birefringence can be *computed* experimentally as (Eq. (2)),

$$\Delta n = \frac{kv}{d}, \tag{2}$$

where k is the fringe order, v, the wavelength of monochromatic light, and d, the depth of sample through which the light propagates. This equation was derived for a homogeneous material, having constant optical properties along the direction of light propagation. In other words, the birefringence is an integrated effect along a

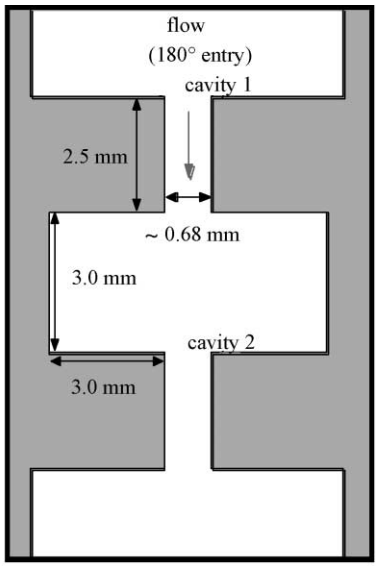

Fig. 4. Schematic diagram of the double-cavity die inserts (grey area). Shown are the slit dimensions (width of the upstream/downstream square cross section, 10.0 mm) and primary flow direction. The entry flow region to the first slit and second slit is denoted as cavity 1 and cavity 2, respectively.

light beam, only birefringence data of two-dimensional fields without birefringence gradients in the propagation direction of the light wave can be translated into stresses by this simple calculation (Baaijens, 1994). In the work described in this paper we are assuming that the flow is two-dimensional and, therefore, the simple interpretation of the birefringence is used. Experimentally, the principal stress difference (PSD), ($|\Delta\sigma|$) can be calculated from the flow birefringence patterns by counting the fringe order (k) and assuming a typical value of C. The stress optical coefficient is essentially independent of deformation rate, molecular weight (MW) and molecular weight distribution (MWD); but is dependent on the monomer unit identity, and mildly on temperature and optical wavelength (see for example, Lodge & Macosko, 1994). For polyethylene melts, the typical value of C is between $+1.2 \times 10^{-9}$ and $+2.4 \times 10^{-9}$ 1/Pa (see for example, Janeschitz-Kriegl, 1983).

3. The MPR, Double Cavity Die (DCD)

The effect of strain history on the rheological response of flowing molten polymer is important (Lee & Mackley, 2000b). This can be effectively studied using the DCD slit configuration in an MPR. A schematic diagram of the double-cavity slit flow region, which was integrated with the optical system in a MPR for flow birefringence observations is shown in Fig. 4. The flow of the material as shown in Fig. 4 is from top to bottom and through two-slits in series that are separated by a middle cavity. The region of entry flow into the first and second slit is denoted as cavity 1 and cavity 2, respectively.

The experiments were carried out for a metallocene based LLDPE melt, m-LLDPE, (melt flow index ~1.0, polydispersity index ~1.99), which is a commercial resin manufactured by the Dow Chemicals. The m-LLDPE is an ethylene alpha-olefin polymer, linear chains with low molecular mass side groups and a small amount of uniformly distributed long chain branching. It is produced using the INSITE Technology from Dow Plastics. Metallocene (single-site) catalysts produce polymers with narrow molecular weight distribution, which in general, results in superior physical and mechanical properties than their Ziegler–Natta counterpart. However, the metallocene polymers can under certain circumstances be difficult to process. The polymer processibility can be improved by introducing long-chain branching (Yan, Wang, & Zhu, 1999).

The overall flow-birefringence pattern for the m-LLDPE at a temperature of 190°C in a steady flow with piston speed of 0.3 mm/s (apparent wall shear rate within the slit ~ 44 1/s) in the DCD, is shown in Fig. 5. In general, the first entry fringe pattern (in cavity 1) had a characteristic '*mushroom*' shape and the second entry fringe pattern (in cavity 2) had a pronounced '*butterfly*' profile. The differences in the entry flow-birefringence profiles indicate that the upstream strain history had modified the subsequent entry flow behaviour in the second slit.

4. Numerical simulation of DCD

In order to numerically simulate the complex flow of the polymer melt in a DCD, a viscoelastic constitutive equation, material characterisation and reliable numerical solver are required.

The K-B.K.Z. integral-type constitutive equation with the irreversible Wagner damping function (Wagner & Laun, 1978; Wagner, 1979), as given in Eq. (3) and a spectrum of relaxation times were used to describe the rheology of the material.

$$\tau(t) = -\int_{-\infty}^{t} \underbrace{\sum_{i=1}^{N} G_i/\lambda_i \exp(-t/\lambda_i)}_{\text{linear memory function}} \times \underbrace{\{\exp[-\kappa\sqrt{\beta I_1 + (1-\beta)I_2 - 3}]\}}_{\text{Wagner damping function}} C^{-1}(t,t')\,\mathrm{d}t', \tag{3}$$

where $\tau(t)$ is the total extra stress tensor, $C^{-1}(t,t')$, the Finger strain tensor that describes the change in shape of a small material element between present and past times, t and t', respectively. In general, the kernel of this equation includes a *time-dependent* linear memory

Fig. 5. Double-cavity flow birefringence patterns of the m-LLDPE at a temperature, 190°C and flow rate, 33.9 mm^3/s (apparent wall shear rate in the slit ~ 44 1/s). Flow is from top to bottom. Comparison of the overall experimental flow birefringence pattern with the simulated PSD (the right hand part of the figure). As seen, the Wagner model simulations captured the fringe pattern at cavity 1 (mushroom shape) and cavity 2 (butterfly shape). The increment of PSD contour lines is 2.95×10^4 Pa (C, 1.74×10^{-9} 1/Pa).

function expressed as a spectrum of relaxation times (G_i, λ_i) and a *strain-dependent* damping function expressed in terms of the first and second scalar invariant, I_1 and I_2, of $C^{-1}(t, t')$.

A standard protocol for establishing rheological data was used to determine material rheological parameters (Mackley, Marshall, Smeulders, & Zhao, 1994) for input in the numerical simulations. Measurements include dynamic viscoelasticity and step-strain stress-relaxation modulus, which can be used to determine the material parameters of this model, a discrete spectrum of relaxation times (G_i, λ_i) and the Wagner damping constant (κ), respectively. Meanwhile, the extensional constitutive parameter, β, was arbitrarily chosen as unity. Nonetheless, β is irrelevant in a planar extension and simple shear flow where both I_1 and I_2 are equal.

For the numerical simulations, a commercial computational fluid dynamics package, POLYFLOW, (Crochet, Debbaut, Keunings, & Marchal, 1992) was used to solve the model (constitutive equations, momentum and incompressibility equations) that describes the physics of the viscoelastic flow of polymer melt in a (simulation) for a flow domain defined by the appropriate experimental flow boundary conditions. The effect of gravity, inertia, viscous heating, compressibility and wall slip were neglected. The flow domain of the DCD is represented by a rectangular element mesh, as shown in Fig. 6. This type of mesh tessellation with refinement along the symmetry plane and in the slit (illustrated in the enlargement) has been found to be effective for numerical convergence. The viscoelastic flow problem was solved in three stages and details of the numerical procedures used can be found in Goublomme, Draily, and Crochet (1992), Ahmed, Liang, and Mackley (1995).

In this paper, we match experimentally obtained flow birefringence with the predictions of numerical simulations for steady state flow conditions. Our optical set-up is not configured to measure explicitly the local shear stress and extinction angle. Therefore, the stress optical coefficient, which is a function of the shear stress, extinction angle and local birefringence, cannot be determined from our experiments that measured only the birefringence. Nevertheless, the value of C was identified by matching the simulated with the calculated *centreline* birefringence data, as shown in Fig. 7. The plot shows a best fit of the simulated PSD to the experimental PSD (Eq. (1)) for the material, with C corresponding to 1.74×10^{-9} 1/Pa, which is within the range obtained for a PE.

Fig. 7 illustrates that the centre line PSD increased rapidly in cavity 1 (material element is stretched as it approaches the slit) and was a maximum at the throat of the slit (denoted by v). Within the slit, the centreline velocity is essentially constant and the centreline PSD rapidly diminishes until just before the exit region is reached. As the polymer melt leaves the slit, the polymer velocity decelerates and material elements are compressed. Thus, in principal the PSD becomes negative and reaches a minimum at the throat of the slit exit (w). However, the experimental technique used does not distinguish the sign of the PSD, so the results shown are interpreted as the magnitude of the PSD. Material elements are not stretched travelling away from the slit and so a decreasing PSD is expected ($w \rightarrow x$). As the second slit is approached, the PSD in cavity 2 increases again to a maximum (y) and subsequently diminish within the slit, and reaches a minimum (z). Subsequently, the stresses diminish in the downstream reservoir.

With the value of C, identified from Fig. 7 the increment of PSD, (v/Cd), was found to be 2.95×10^4 Pa.

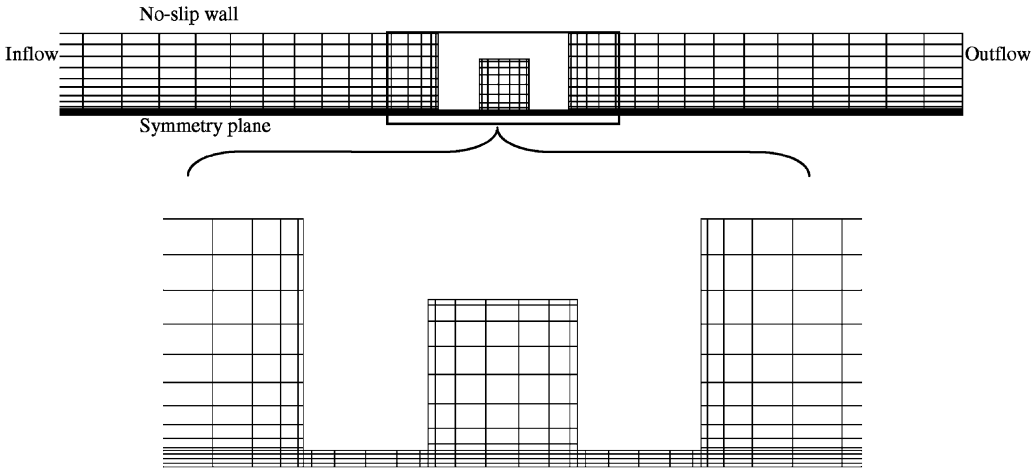

Fig. 6. Finite-element mesh with a symmetry plane representing the flow domain in the double-cavity slit. Enlargement of the middle section shows the mesh tessellation along the centreline/symmetry plane and refinement in the slit.

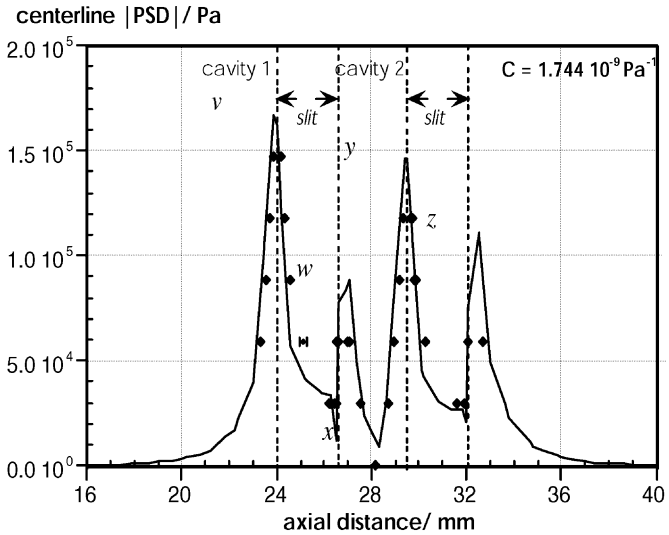

Fig. 7. Comparison between the experimental (•) and predicted (—) steady state centreline PSD for the m-LLDPE material for the flow conditions as described in Fig. 5.

This increment can be specified within *Polyplot* (results post-processor in POLYFLOW) to plot the contour lines of the PSD field, as seen on the right hand part of Fig. 5. The simulation captured the differences between the fringe patterns in the upstream entry into the first slit (cavity 1) and the entry into the second slit (cavity 2), at least qualitatively. Furthermore, at a distance of approximately one-third from the slit entrance (downstream of both cavities), the fringes within both slit lands straighten out and are parallel to the slit wall, and thus represent a fully developed flow region. The K-B.K.Z.–Wagner numerical simulations was, therefore, able to successfully predict the significant differences in the stress field that were seen experimentally, demonstrating the effect that past strain history can have on flow behaviour.

5. Discussions and conclusions

We have demonstrated the application of a MPR for the rheo-optic study of a PE melt in a double-cavity slit die configuration. In particular, the effect of strain history on the flow behaviour of PE was revealed using this geometry in terms of differences in the observed stress field for the two cavities. We have found that the fully

constrained geometry of the double piston MPR enables many systematic experiments to be carried out on a small quantity of polymer. The optic cell attachment also enables flow birefringence studies to be made for small quantities of material. The geometries chosen are close to that of processing flows and in addition the MPR is capable of generating shear rates that are also typical for commercial practise. Using this apparatus and the techniques described in this paper it should be possible, in the future to use the MPR as a sensitive laboratory tool for exploring the processing response of polymers having different molecular architectures. In addition the MPR can be used to rank the performance of viscoelastic numerical simulations.

Acknowledgements

We have pleasure in dedicating this paper to Dr. R.A. Mashelkar in recognition of his prolific and significant contribution to the field of polymer science. K.L. is also grateful for financial support from the Commission of European Union through a BRITE-EURAM III ART Project (BE96-3490). MRM would like to thank CRNS and CEMEF Sophia Antipolis for the opportunity to help prepare this paper whilst working in France.

References

Ahmed, R., Liang, R. F., & Mackley, M. R. (1995). The experimental observation and numerical prediction of planar entry flow and die swell for molten polyethylene. *Journal of Non-Newtonian Fluid Mechanics*, *59*, 129–153.

Baaijens, F. P. T., Verbeeten, W. M. H., & Peters, G. W. M. (2000). Analysis of viscoelastic polymer melt flow. *Proceedings of the XIIIth international congress on rheology*, Cambridge, U.K.

Baaijens, H. P. W. (1994). *Evaluation of constitutive equations for polymer melts and solutions in complex flows*. Ph.D. thesis, Eindhoven University of Technology, The Netherlands.

Cheng, Y. K., Mackley, M. R., & Sayer, T. (2000). Colour rheology measurements and its link to microstructural change. In D. M. Binding, N. E. Hudson, J. Mewis, J. M. Piau, C. J. S. Petrie, P. Townsend, & M. Wagner (Eds.), *Proceedings of the XIII international congress on rheology*. Cambridge, vol. 3. Glasgow: BRS (pp. 40–42).

Chowdhury, J., & Moore, S. (1993). Polymers by blueprint. *Chemical Engineering*, 34–39.

Crochet, M. J., Debbaut, B., Keunings, R., & Marchal, J. M. (1992). POLYFLOW: A multi-purpose finite element program for continuous polymer flows. In K. T. O'Brien (Ed.), *Applications of CAE in extrusion and other continuous processes*. Munich: Carl Hanser Verlag (pp. 25–50) (Chapter 2).

Dealy, J. M. (1998). Flow instabilities as stress limiters for molten polymers. *Proceedings of the fifth european rheology conference*, *progress and trends in rheology*, *Portoroz*, *Slovenia*. Germany: Springer.

Engmann, J., & Mackley, M. R. (2000). Changes in microstructure and rheological behaviour of chocolate during extrusion. In D. M. Binding, N. E. Hudson, J. Mewis, J. M. Piau, C. J. S. Petrie, P. Townsend, & M. Wagner (Eds.), *Proceedings of the XIIIth international congress on rheology*, Cambridge. vol. 4. Glasgow: BRS (pp. 368–370).

Goublomme, A., Draily, B., & Crochet, M. J. (1992). Numerical prediction of extrudate swell of a high-density polyethylene. *Journal of Non-Newtonian Fluid Mechanics*, *44*, 171–195.

Janeschitz-Kriegl, H. (1983). *Polymer melt rheology and flow birefringence*. Berlin: Springer.

Koopmans, R. J. (1993). Extrudate swell of high density polyethylene, part I: Aspects of molecular structure and rheological characterization methods; Part II: Time dependency and effects of cooling and sagging. *Polymer Engineering Sciences*, *32*, 1741.

Lee, K., & Mackley, M. R. (2000a). The significance of slip in matching polyethylene processing data with numerical simulation. *Journal of Non-Newtonian Fluid Mechanics*, *94*, 159–177.

Lee, K., & Mackley, M. R. (2000b). The effect of strain history on the entry flow of polyethylene. In D. M. Binding, N. E. Hudson, J. Mewis, J. M. Piau, C. J. S. Petrie, P. Townsend, & M. Wagner (Eds.), *Proceedings of the XIIIth international congress on rheology*, Cambridge, vol. 1. Glasgow: BRS (pp. 115–117).

Lodge, T. P., & Macosko, C. W. (1994). Rheology, principles, measurements and applications. *Rheo-optics*: *Flow birefringence*. (1st ed.) Weinheim: VCH Publisher, Inc., (Chapter 9).

Mackley, M. R., & Spitteler, P. H. J. (1996). Experimental observations on the pressure-dependent polymer melt rheology of linear low density polyethylene using a multi-pass rheometer. *Rheologica Acta*, *35*, 202–209.

Mackley, M. R., & Thompson, M. J. (2000). The low and high shear rheology of emulsions of water in alkyd resin as a model for lithographic printing inks. In D. M. Binding, N. E. Hudson, J. Mewis, J. M. Piau, C. J. S. Petrie, P. Townsend, & M. Wagner (Eds.), *Proceedings of the XIIIth international congress on rheology*, Cambridge, vol. 3. Glasgow: BRS (pp. 279–281).

Mackley, M. R., Marshall, R. T. J., & Smeulders, J. B. A. F. (1995). The multipass rheometer. *Journal of Rheology*, *39*(6), 1293–1309.

Mackley, M. R., Marshall, R. T. J., Smeulders, J. B. A. F., & Zhao, F. D. (1994). The rheological characterisation of polymeric and colloidal fluids. *Chemical Engineering Sciences*, *49*, 2551–2565.

Mackley, M. R., Moggridge, G. D., & Saquet, O. (2000). Direct experimental evidence for the preferential growth of flow induced fibrous polymer crystallisation occurring at a solid/melt interface. *Journal of Material Science*, *35*(20), 5247–5254.

Martino, R. (1992). New polyolefin resins emerge: 'branched linear' copolymers. *Modern Plastics International*, *November*, 16–18.

Ranganathan, M., Mackley, M. R., & Spitteler, P. H. J. (1999). The transient rheology and processing of polyethylene melts. *Journal of Rheology*, *43*, 443–451.

Reade, L. (1995). Metallocenes: The market for Metallocenes, Who's doing What?, Leaving the Lab, in European Plastics News, June, 23, 24, pp. 26–27.

Schoonen, J. F. M. (1998). *Determination of rheological constitutive equations using complex flows*. Ph.D. thesis, Eindhoven University of Technology, The Netherlands.

Thompson, M. J., Mackley, M. R., & Nimmo, J. A. (2000). The high shear rheology of lithographic emulsions. *Surface Coatings International*, *83*(5), 234–239.

Wagner, M. H. (1979). Analysis of time dependant stress growth data for shear and elongational flow of a low density polyethylene. *Rheologica Acta*, *18*, 33–55.

Wagner, M. H., & Laun, H. M. (1978). Non-linear shear creep and constrained elastic recovery of a LDPE melt. *Rheologica Acta*, *17*, 138–148.

Wales, J. L. S. (1976). *The application of flow birefringence to rheological studies of polymer melts*. (PhD thesis), Technische Hogeschool Delft, The Netherlands.

Wee, W.-K., & Mackley, M. R. (1998). The rheology and processing of a concentrated Cellulose Acetate solution. *Chemical Engineering Sciences*, *53*(6), 1131–1144.

Yan, D., Wang, W.-J., & Zhu, S. (1999). Effect of long chain branching on rheological properties of metallocene polyethylene. *Polymer*, *40*, 1737–1744.